Coexistence of antiferromagnetism and ferromagnetism in $Ca_{1-x}Pr_xMnO_3$ ($x \leqslant 0.1$) manganites

M. M. Savosta
Donetsk Institute of Physics & Technics, Academy of Sciences of Ukraine, Rozy Luxembourg 72, 83114 Donetsk, Ukraine

P. Novák, M. Maryško, Z. Jirák, and J. Hejtmánek
Institute of Physics, Academy of Sciences of the Czech Republic, Na Slovance 2, 182 21 Praha 8, Czech Republic

J. Englich and J. Kohout
Faculty of Mathematics & Physics, Charles University, V Holešovičkách 2, 180 00 Praha 8, Czech Republic

C. Martin and B. Raveau
Laboratoire CRISMAT, UMR 6508, ISMRA, Boulevard du Maréchal Juin, 14050 Caen, France
(Received 1 June 2000)

The magnetism in three polycrystalline samples of the electron doped manganites $Ca_{1-x}Pr_xMnO_3$ ($x = 0.025, 0.05, 0.1$) was investigated by NMR on ^{55}Mn and ^{141}Pr nuclei, neutron diffraction, and magnetic measurements. In all systems the coexistence of majority antiferromagnetic and minority ferromagnetic phases was found. At 4.2 K distinct NMR signals from ferromagnetic domains and antiferromagnetic matrix as well as from the domain walls were detected. Magnetic moment at 4.2 K increases sharply with increasing x from $0.06\mu_B$ pfu ($x=0.025$) to $0.9\mu_B$ pfu ($x=0.1$) accompanied by an equally sharp increase of the ferromagnetic NMR signal. For the $x=0.1$ sample the temperature dependence of the ferromagnetic moment determined by neutrons and NMR agrees well with the magnetic measurements. For smaller x the NMR gives essentially the same dependence, while the bulk magnetization decreases with increasing temperature more rapidly, indicating reduction of the ferromagnetic volume when temperature is raised. For a more complete characterization of the system studied the temperature dependencies of the electrical resistivity and thermopower were also measured.

I. INTRODUCTION

The hole doped manganite perovskites $A_{1-x}R_xMnO_3$ ($x \rightarrow 1$, R is trivalent rare-earth ion, A is divalent or monovalent cation) were subject of numerous studies, in connection with the ''colossal'' magnetoresistivity observed in these systems. Systems with $x \approx 0.5$ are also of considerable interest. Due to the competition of several interactions—antiferromagnetic superexchange, ferromagnetic double exchange, charge ordering, and Jahn-Teller effect of Mn^{3+} ion—a strong tendency to the phase separation exists here (see Ref. 1 for a recent survey).

Much less is known about the electron doped region ($x \rightarrow 0$). Pure $CaMnO_3$ is a G-type antiferromagnet ($T_N = 123$ K) with a weak canting of about 0.3°.[2] When part of Ca is substituted by a trivalent cation a more marked ferromagnetic component develops, however. Maignan *et al.*[3] found that in a number of $Ca_{1-x}R_xMnO_3$ manganites this component increases with increasing x, reaches its maximum of about $1\mu_B$ pfu for $x \sim 0.1$, and rapidly disappears when x is further increased. The nature of the ferromagnetic component is far from being clear—it has been explained as due to the canted antiferromagnetism,[4] cluster glass state,[5] or by ferromagnetic domains embedded in the antiferromagnetic matrix.[6] NMR is a suitable tool allowing one to decide unambiguously between these possibilities (see, e.g., Ref. 7).

In the present paper we give the results of the NMR study of three $Ca_{1-x}Pr_xMnO_3$ manganites ($x = 0.025, 0.05, 0.1$) and compare them to the neutron-diffraction and magnetization data. The system is further characterized by measurements of the magnetic susceptibility, electrical resistivity, and thermopower.

II. EXPERIMENTAL DETAILS

The ceramic samples were prepared from mixtures of CaO, Pr_2O_3, and MnO_2 preheated at 1000 °C in air, pressed into the form of bars, heated at 1200 °C, and then sintered for 12 h at 1500 °C. The purity, homogeneity, and composition of the samples were checked by x-ray diffraction, electron diffraction, and energy dispersive spectroscopy (EDS) analysis. Complete neutron-diffraction data on the crystal structure and magnetic arrangement of the composition $x = 0.1$ are reported in Ref. 6. It appears that the ferromagnetic and antiferromagnetic temperatures coincide; $T_C = T_N = 110$ K.

The measurements of the dc magnetization and ac susceptibility were carried out using the Quantum Design superconducting quantum interference device (SQUID) magnetometer. The magnetization was measured in fields up to 5 T and the spontaneous moment was then determined by extrapolating the data to zero magnetic field. The electric conductivity was measured by a standard four-probe method and the thermopower was studied using a steady-state four-probe technique with a constant gradient ~ 1 K.

The NMR spectra were recorded by a two-pulse spin-echo method at temperatures between 61 and 100 K using a noncoherent spectrometer with frequency sweep and boxcar de-

 ©2000 The American Physical Society

tector signal averaging. The measurements at 4.2 K and for selected cases also at 77 K were performed on phase-coherent spectrometer with an averaging technique and the complex Fourier transformation using an untuned probe head. In the latter case the spectra were measured recording point by point the Fourier amplitude of the echo signal varying the transmitter frequency, the upper limit for the frequency was 300 MHz. All the samples in question are conducting. For this reason, when comparing the amplitudes of NMR signal in different samples, we used powders fixed in the paraffin.

In the magnetic systems the action of an external magnetic field B_{ext} on the nuclear spins is magnified by the hyperfine coupling (interaction of the nuclear spin with the electronic magnetic moment). This enhancement concerns both the static component of B_{ext} and its radiofrequency component B_{rf}. The corresponding enhancement factor η, defined as a ratio of the time-dependent component b_{eff} of the effective hyperfine field to B_{rf}, is to a good approximation proportional to local susceptibility of the electronic system. The maximum amplitude of the spin-echo signal is obtained when $b_{eff}=\eta B_{rf}$ reaches the value which turns the nuclear magnetization by an angle $\pi/2$. This fact allows us to differentiate between NMR signals which occur at the same frequency, but arise from regions possessing different local susceptibility and therefore different η. In the systems in question we are thus able to distinguish the signal from the nuclei in the domain walls (η larger than 10^4) from the signals of nuclei in the ferromagnetic domains (η of the order 10^2) and antiferromagnetic domains (smallest susceptibility, $\eta \leqslant 20$). To this end we study the dependence of the spin-echo amplitude on the value of the rf field at the given frequency and with fixed length of the pulses. The first maximum on this dependence corresponds to rf field for which the optimum excitation conditions are fulfilled for nuclei in the regions with the largest η (domain walls). The antiferromagnetic regions, in which it is most difficult to excite the nuclear spins, would correspond to the last maximum. In fact, in the latter case, even with the largest rf power available and with longer pulses, we were not able to reach the optimum excitation conditions.

III. RESULTS

The temperature dependencies of the inverse susceptibility, electrical resistivity, and thermoelectric power in Fig. 1 provide a basic physical characterization of the samples under study. For comparison the data obtained on a pure $CaMnO_3$ sample with almost ideal oxygen stoichiometry are also given. The samples $x=0.1$, 0.05, and 0.025 are essentially conducting in paramagnetic state and exhibit the same magnetic critical temperature of 110 K. Nonetheless the asymptotic paramagnetic temperature θ shifts gradually towards negative temperatures. Pure $CaMnO_3$ displays a semiconducting character (activation energy $E_A \sim 0.06$ eV) and strong antiferromagnetic interaction evidenced by $\theta \approx -600$ K. This sample has $T_N=123$ K and possesses a weak net moment of $0.027\mu_B$ per f.u. as it was determined by the magnetization measurements.

The linear temperature dependence of thermoelectric power observed in the paramagnetic state for both the Pr

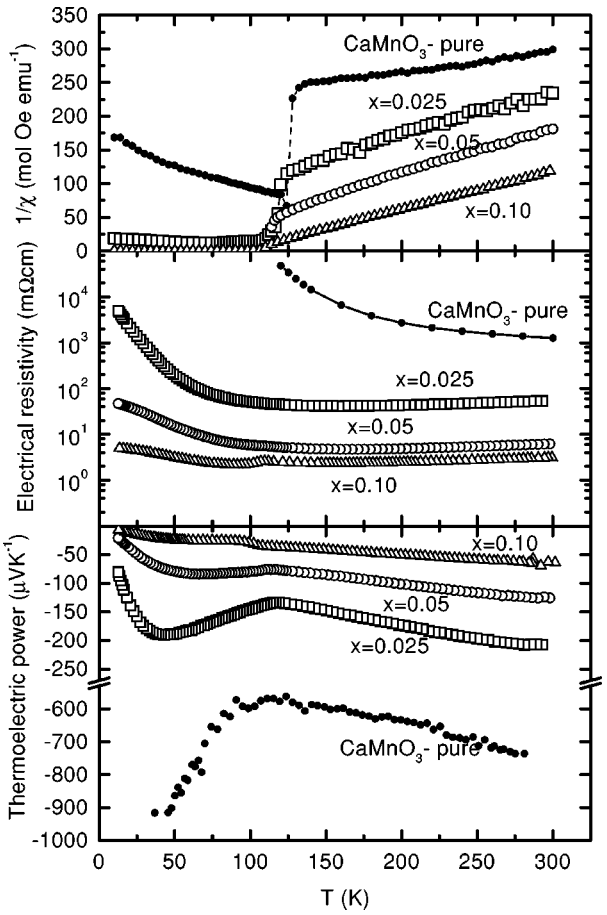

FIG. 1. Temperature dependence of inverse susceptibility (upper panel), electrical resistivity (middle panel), and thermopower (lower panel) in the $Ca_{1-x}Pr_xMnO_3$ system ($0 \leqslant x \leqslant 0.1$).

substituted samples and $CaMnO_3$ is a characteristic feature of metallic conductivity. Consequently we infer that the charge carriers are essentially itinerant, irrespective of doping. In frame of such picture the increasing slope of thermopower reflects the decreasing carrier (electron) concentration and scales well with chemical composition, i.e., with decreasing Pr content. For pure $CaMnO_3$ the carrier concentration is evidently very low and chemical determination is impossible. Using the thermopower data we can, however, estimate the electron concentration on a base of the linear temperature dependence of thermoelectric power below 300 K to ~ 0.01 electron per Mn. The apparent discrepancy between the metallic behavior of thermopower and the above-mentioned semiconducting resistivity in $CaMnO_3$ might be explained by the drop of Fermi level E_F just below the mobility edge E_μ. This is a consequence of both disorder, which leads to creation of localized states at the band edge, and of a low filling of the band.[8]

NMR spectra detected at liquid-He temperature are displayed in Figs. 2 and 3. In all three samples five approximately equidistant lines, the amplitude of which increases with the Pr concentration, were observed (Fig. 2). We ascribe these lines to the quadrupole split resonance of the ^{141}Pr nuclei ($I=5/2$). The ^{55}Mn NMR spectrum consists of two distinct features centered around 245 and 300 MHz in all three samples [Fig. 3(a)]. The NMR signal at ≈ 300 MHz possesses large enhancement factor $\eta \approx 200-400$, which is

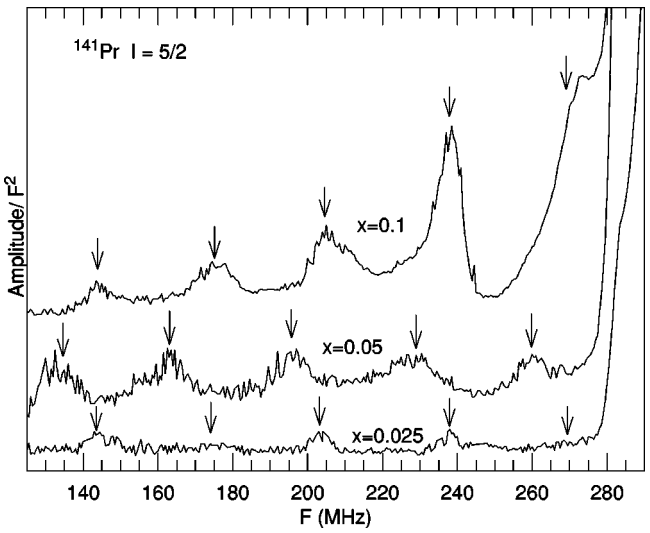

FIG. 2. NMR spectra of ^{141}Pr in $Ca_{1-x}Pr_xMnO_3$ perovskites at the liquid-He temperature. The arrows point to the centers of individual Pr lines.

characteristic for a ferromagnetic (FM) phase, while the line at 245 MHz has much smaller enhancement $\eta \leqslant 20$, indicating that it arises from an antiferromagnetic (AFM) phase. We note that a similar NMR spectrum of ^{55}Mn, with the same assignment, was observed by Allodi *et al.*[7] in $La_{0.5}Ca_{0.5}MnO_3$. The enhancement factor of ^{141}Pr lines is the same as the one of FM ^{55}Mn, suggesting that the Pr

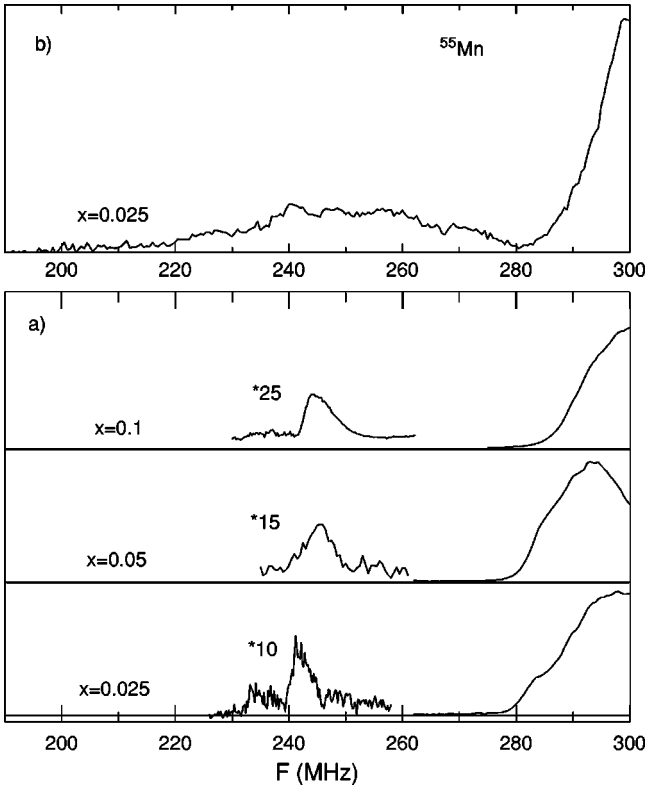

FIG. 3. NMR spectra of ^{55}Mn in $Ca_{1-x}Pr_xMnO_3$ perovskites at the liquid-He temperature. (a) Nuclei inside the domains. The signals arising from the AFM domains were magnified by factor 10 ($x=0.0025$), 15 ($x=0.05$), and 25 ($x=0.1$), in order to make them better visible. (b) Nuclei in the domain walls.

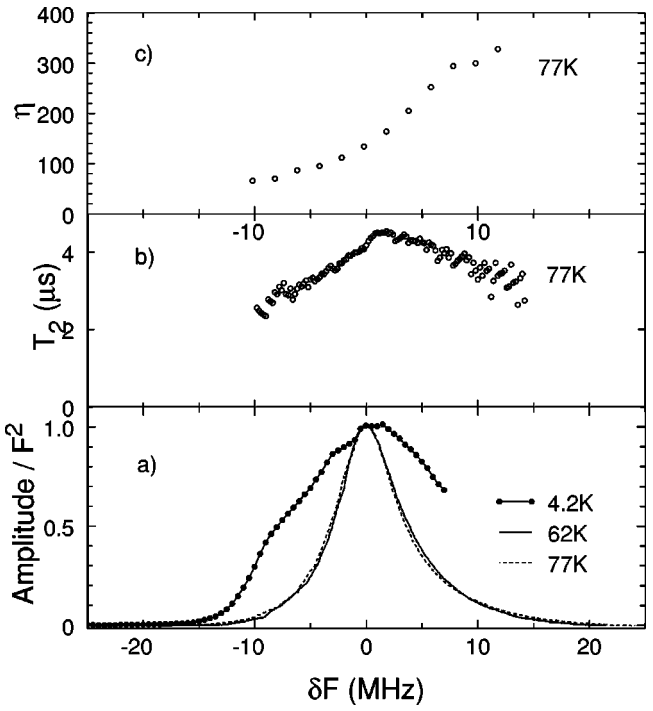

FIG. 4. $Ca_{0.95}Pr_{0.05}MnO_3$. (a) NMR spectra of ^{55}Mn in the FM domains at three different temperatures. To compare their form the spectra were normalized and shifted so that their maxima coincide $\delta F = F - F_{max}$. (b) $T=77$ K. Spin-spin relaxation time T_2 as a function of frequency (rf field 1.5 G and 1-μs pulses were used). (c) $T=77$ K. Enhancement factor η as a function of frequency.

resonance arises from the nuclei in the ferromagnetic phase. In addition a broad resonance, having two maxima, is observed [Fig. 3(b)], when the level of radiofrequency field is very low ($\eta \approx 20\,000$), which we ascribe to the ^{55}Mn domain-wall signal.

For the discussion in the subsequent section, the NMR arising from the nuclei in the domains is important and on it we now focus our attention. As seen in Fig. 3(a), at $T=4.2$ K the spectrum of ^{55}Mn nuclei in the FM domains is broad, consisting probably of several lines. At higher temperatures it narrows and its structure disappears [Fig. 4(a)]. In Fig. 5(a) this spectrum at $T=63$ K, corrected for the transverse relaxation and enhancement factor, is compared

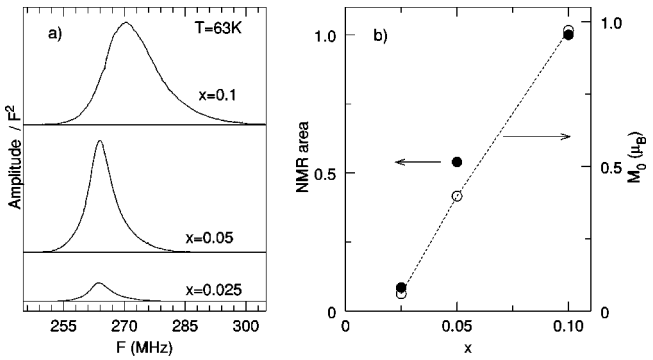

FIG. 5. $Ca_{1-x}Pr_xMnO_3$ perovskites at 63 K. Comparison of the FM NMR spectra of ^{55}Mn for three compositions (a), and dependence of the NMR signal area and the spontaneous magnetic moment pfu M_0 on x (b).

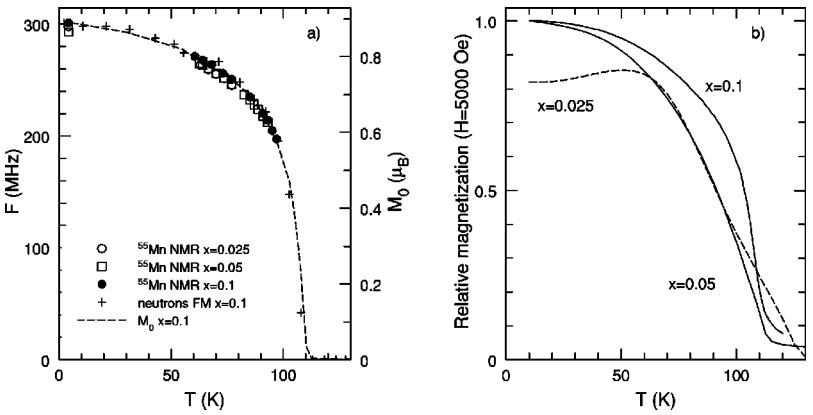

FIG. 6. Temperature dependence of the resonance frequency of ^{55}Mn NMR in the FM phase in $Ca_{1-x}Pr_xMnO_3$. For the $x=0.1$ sample the temperature dependence of the magnetic moment determined from neutron scattering and magnetic measurements is also shown (a). Magnetization vs temperature for $Ca_{1-x}Pr_xMnO_3$ manganites in an applied magnetic field of 0.5 T (b).

for the three Pr concentrations x. The area of the NMR spectrum sharply increases with x and it correlates well with the increase of the magnetic moment as determined from the magnetic measurements [Fig. 5(b)]. This provides an additional confirmation of the assignment of this spectrum to the FM phase.

The temperature dependence of the NMR frequency of the FM signal $F(T)$, displayed in Fig. 6(a), has the same form for all three concentrations of Pr. Also in Fig. 6(a), the temperature dependence $M(T)$ of the spontaneous FM moment for $x=0.1$ sample, as determined by magnetic measurements and neutron diffraction,[6] is shown. It is seen that all these dependencies coincide. In Fig. 6(b) the $M(T)$ dependencies at $B=0.5$ T are compared for $x=0.025$, 0.05, and 0.1 samples. Unlike the $F(T)$ curves the dependencies of the magnetization are different for different x.

IV. DISCUSSION

A. Magnetic moment of Pr^{3+} ion

^{141}Pr nuclei has nuclear spin $I=5/2$. The splitting of the nuclear levels is described by an effective Hamiltonian H_{eff}, consisting of the magnetic hyperfine interaction proportional to an effective magnetic field $\vec{B}_{eff}$, and the hyperfine quadrupolar interaction proportional to P_{eff}:

$$H_{eff}=-g_n\beta_n(\vec{B}_{eff}\vec{I})+P_{eff}[3I_z^2-I(I+1)+\eta_a(I_x^2-I_y^2)]. \quad (1)$$

η_a $(0\leqslant\eta_a\leqslant 1)$ is the parameter describing the deviation from the axial symmetry. As seen in Fig. 2 five lines corresponding to the ^{141}Pr NMR are to a good approximation equidistant, which indicates that in Eq. (1) the magnetic hyperfine interaction dominates and the first-order perturbation theory may be applied. From the position of the lines we then obtain

$$-g_n\beta_nB_{eff}=200(5)\ \text{MHz};\quad P_{eff}=6.0(5)\ \text{MHz}. \quad (2)$$

The effective magnetic field is simply related to the hyperfine coupling constant A_J,

$$-g_n\beta_nB_{eff}=A_J\langle J_z\rangle, \quad (3)$$

where $\langle J_z\rangle$ is the average value of the total angular momentum. The electronic magnetic moment of the praseodymium ion is

$$m_{\mathrm{Pr}}=g_J\mu_B\langle J_z\rangle. \quad (4)$$

The ground state of the Pr^{3+} ion is $^3H_4$ and corresponding factor $g_J=4/5$. Taking for the hyperfine coupling constant the value $A_J=+1093(10)$ MHz[9] we obtain $m_{\mathrm{Pr}}=0.150(7)\mu_B$.

B. Form of the ^{55}Mn NMR at low temperatures

At 4.2 K [Fig. 3(a)] the AFM resonance is relatively narrow (the width in the half amplitude $\Delta F\approx 5$ MHz), while the FM resonance is broad ($\Delta F\approx 15$–20 MHz) and it exhibits an unresolved structure. When temperature is increased, FM resonance narrows substantially to 6, 7, and 13 MHz for $x=0.025$, 0.05, and 0.1, respectively. For $x=0.05$ this is documented in Fig. 4(a). The structure of FM line, observed at 4.2 K, can be explained as a result of the quadrupole splitting of the ^{55}Mn resonance ($I=5/2$). In the presence of the quadrupolar splitting the Redfield theory predicts that the nuclear relaxation cannot be described by a single exponential.[10] Indeed, we have found that the spin-lattice relaxation has a multiexponential character here, in distinction to the AFM line (Fig. 7). Besides, the relaxation becomes single exponential when the temperature is raised. The appearance of the quadrupole splitting can be associated with the ordering of the Pr^{3+} electronic magnetic moments in the FM phase. No such ordering is probable in the AFM phase, as the effective exchange fields on Pr^{3+} from its Mn neighbors cancel. Combined effect of the spin polarization, crystal field, and spin-orbit coupling leads to a nonspherical electron density on the Pr^{3+} ion, which may give rise to the electron field gradient on nearest manganese neighbors, e.g., via the local magnetostriction. When the temperature is increased, the Pr^{3+} magnetic moment is expected to decrease rapidly[11] and therefore the quadrupole splitting on ^{55}Mn diminishes.

To confirm our interpretation we measured the NMR at $T=4.2$ K also on the lanthanum analog of the $x=0.05$ sample, $Ca_{0.95}La_{0.05}MnO_3$. As expected, AFM and FM ^{55}Mn spectra of comparable width were detected ($F\approx 240$ and 290 MHz) and the FM signal exhibited no structure. These results will be published elsewhere.

C. Characterization of the magnetic phases

As mentioned in the Introduction, the magnetic moment of the system in question may be ascribed either to a single

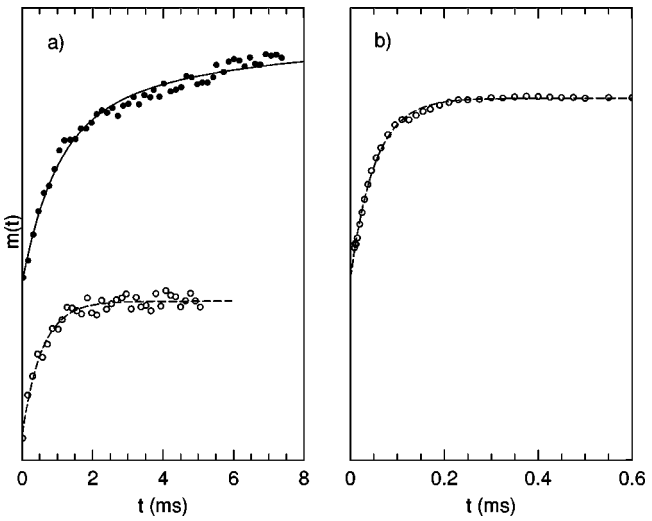

FIG. 7. $Ca_{0.95}Pr_{0.05}MnO_3$. Decay of the longitudinal component of the Mn nuclear magnetization $m(t)$ in (a) AFM (○) and FM (●) phases at 4.2 K and (b) FM phase at 77 K. The decays in the AFM phase and in the FM phase at 77 K are well described by the single exponential with $T_1=0.56$ and 0.052 ms, respectively (dashed curves), while the decay in the FM phase at 4.2 K is multiexponential and the Redfield theory is used to fit it (full curve).

phase with small magnitude of the ferromagnetic moment (canted AFM or spin glass) or as a mixture of AFM and FM phases. In the former case there should be single NMR spectrum of ^{55}Mn as all the lattice sites occupied by Mn are equivalent. We observed two distinct spectra of ^{55}Mn, which clearly demonstrates that the second possibility is realized—the system consists of the mixture of FM and AFM phases. The area of NMR spectra of ^{55}Mn in the FM phase increases sharply with increasing concentration of Pr indicating that the volume of FM phase increases. Correspondence of this area with the magnetization data [Fig. 5(b)] shows that the increase of the bulk magnetic moment reflects the growth of the FM phase with x.

Disregarding the quadrupole interaction and small dipolar contributions, the hyperfine field on the ^{55}Mn nuclei may be written as

$$\vec{B}_{eff}=g_n\mu_B\hat{A}\vec{S}+g_n\mu_B\sum_{i=1}^{6}\hat{a}\vec{S}_i. \qquad (5)$$

The first term corresponds to the on-site contribution, $\hat{A}$ is the magnetic hyperfine coupling tensor, $\vec{S}$ is the electronic spin of the Mn ion in question. The second term is the field transferred from the six nearest Mn neighbors having the spin $\vec{S}_i$, $\hat{a}$ is the transferred magnetic hyperfine tensor. The NMR frequency is connected with $\vec{B}_{eff}$ by

$$F=\gamma|\vec{B}_{eff}|/2\pi. \qquad (6)$$

Equations (5) and (6) predict different resonance frequencies for FM and AFM as the transferred term in Eq. (5) has the opposite sign in the FM and the G-type AFM spin arrangements.

The mean valency of the Mn ions in the system studied is slightly less than 4. Previous NMR studies of ferromagnetic Mn perovskites[12–15] have shown that at low temperatures the Mn^{4+} and Mn^{3+} spectra occur at 310–330 MHz and 400–420 MHz, respectively. The FM line in present samples lies somewhat lower than expected from this picture. If we assume that the anisotropy of $\vec{B}_{eff}$ is small, this difference may be explained by a change in the magnitude of the hyperfine coupling constant [Eq. (5)] or by a larger hybridization of the manganese $3d$ and oxygen $2p$ states, as indicated by calculation of Pickett and Singh.[16]

The signal from nuclei in the domain walls also deserves a short comment. It consists of two broad peaks centered around AFM domain and FM domain spectra, respectively. These two signals have different relaxation times T_1 and T_2 and we tentatively ascribe them to domain walls in the AFM and FM phase, respectively. The AFM domain-wall signal observed at 4.2 K is very broad, which shows that a large distribution of B_{eff} in the AFM walls exists. On the other hand the signal from the FM domain walls, observed in broad temperature interval, differs only slightly from the FM domain signal—it is slightly broader and shifted by ≈ 5 MHz to higher frequencies.

From Fig. 6(a) follows that the temperature dependence of F is the same in the three samples studied. F is proportional to the magnetic moment of the manganese ion [Eqs. (5) and (6)], the comparison of NMR and magnetic measurements then allows us to obtain the FM phase volume as a function of temperature. In the $x=0.1$ sample the NMR, neutron, and magnetic data fall on the same curve [Fig. 6(a)], which shows that the minority FM phase is stable in the whole temperature range. For smaller concentration of Pr the situation is different. As seen from Fig. 6(b) for $x=0.05$ the magnetization decreases faster with increasing temperature comparing to $x=0.1$. As the NMR data give the same temperature dependence of Mn magnetic moment, this means that for $x=0.05$ the FM phase is not stable and volume of this phase continuously decreases. The situation is still more complex for the $x=0.025$ sample. Above 100 K the $M(T)$ dependence exhibits a tail, which can be ascribed to a presence of the antiferromagnetic $CaMnO_3$-type phase with the critical temperature ≈ 123 K. Below 60 K the slight decrease of M is probably connected with the transformation of the part of FM domains into the AFM state.

In addition, there are several indications that the FM phase in the $x=0.025$ and 0.05 samples is very inhomogeneous. The form of the narrowed FM signal seems to be simple [Fig. 5(a)], however, it depends on the excitations conditions and also the relaxation changes substantially throughout the line. This can be understood if the spectrum consists of several signals at close resonance frequencies, but distinct properties. Shown in Figs. 4(b) and (c) are the enhancement factor and spin-spin relaxation time through the FM domain spectrum for $x=0.05$ sample at $T=77$ K. We also observed that the enhancement factor decreases with increasing temperature. These features differ from what we have observed in more conventional FM manganites[17] and they may be tentatively associated with the manganese nuclei in the FM domains of different size and morphology. We note that in the $x=0.1$ these features are also present, though they are much weaker.

In a recent paper[18] the effect of the electron doping on the magnetic moment in $Ca_{1-x}La_xMnO_3$ ($0\leqslant x\leqslant 0.2$) system

was studied. The results for $x<0.08$ are explained through a phenomenological model in which the existence of local ferromagnetic regions within the antiferromagnetic host is assumed. The results we present here provide a justification of such assumption.

V. CONCLUSIONS

We showed that the magnetic state of the electron doped manganites $Ca_{1-x}Pr_xMnO_3$ is phase separated, consisting of ferromagnetic domains embedded in the antiferromagnetic matrix. For $x=0.1$ the FM phase is stable in the whole temperature region of its existence and the temperature dependencies of the magnetic moment obtained by NMR, neutron diffraction, and magnetic measurement coincide. For smaller x the ferromagnetism becomes unstable, its volume decreases as the temperature is increased.

ACKNOWLEDGMENTS

The authors acknowledge discussions with S. Krupička. This work was supported by Grant Nos. 202/99/0413 and 202/00/1601 of the Grant Agency of the Czech Republic.

[1] A. Moreo, S. Yunoki, and E. Dagotto, Science **283**, 2034 (1999).
[2] V.M. Yudin, A.I. Gavrilishina, M.V. Artemeva, and M.F. Bryzhina, Fiz. Tverd. Tela (Leningrad) **7**, 2292 (1965) [Sov. Phys. Solid State **7**, 1856 (1965)].
[3] A. Maignan, C. Martin, F. Damay, and B. Raveau, Chem. Mater. **10**, 950 (1998).
[4] K. Hagdorn, D. Hohlwein, J. Ihringer, K. Knorr, W. Prandl, H. Ritter, H. Schmid, and Th. Zeiske, Eur. Phys. J. B **11**, 243 (1999).
[5] A. Maignan, C. Martin, F. Damay, B. Raveau, and J. Hejtmánek, Phys. Rev. B **58**, 2758 (1998).
[6] C. Martin, A. Maignan, M. Hervieu, and B. Raveau, Phys. Rev. B **60**, 12 191 (1999).
[7] G. Allodi, R. De Renzi, F. Licci, and M.W. Pieper, Phys. Rev. Lett. **81**, 4736 (1998).
[8] N. Mott and E.A. Davis, *Electronic Processes in Non-Crystalline Materials*, 2nd ed. (Clarendon Press, Oxford, 1979).
[9] A. Abragam and B. Bleaney, *Electron Paramagnetic Resonance of Transition Ions* (Clarendon Press, Oxford, 1970).
[10] E.R. Andrew and D.P. Tunstall, Proc. Phys. Soc. London **78**, 1 (1961).
[11] Z. Jirák, S. Vratislav, and J. Zajíček, Phys. Status Solidi A **52**, K39 (1979).
[12] G. Matsumoto, J. Phys. Soc. Jpn. **29**, 615 (1970).
[13] L.K. Leung and A.H. Morish, Phys. Rev. B **15**, 2485 (1977).
[14] A. Anane, C. Dupas, K. LeDang, J.P. Renard, P. Veillet, A.M. deLeonGuevara, F. Millot, L. Pinsard, and A. Revcolevschi, J. Phys.: Condens. Matter **7**, 7015 (1995).
[15] G.J. Tomka, P.C. Riedi, Cz. Kapusta, G. Balakrishnan, D.McK. Paul, M.R. Lees, and J. Barratt, J. Appl. Phys. **83**, 7151 (1998).
[16] W.E. Pickett and D.J. Singh, Phys. Rev. B **53**, 1146 (1996).
[17] M.M. Savosta, V.A. Borodin, and P. Novák, Phys. Rev. B **59**, 8778 (1999).
[18] J.J. Neumeier and J.L. Cohn, Phys. Rev. B **61**, 14 319 (2000).